DOI:10.31557/APJCC.2026.11.6.917

RESEARCH ARTICLE

An Empirically Derived Seven-Gene Immune Prognostic Signature Enriched in T-Cell Exhaustion Mediators Stratifies Survival Outcomes in HPV-Positive and HPV-Negative Head and Neck Squamous Cell Carcinoma

Sharjeel Chaudhry[1]*, Zarmina Ehtesham[1], Fatimah Salem Alayidh[2]

[1]Department of Molecular Pathology, Dow Diagnostic Research and Reference Laboratory, Dow University of Health Sciences, Karachi, Pakistan. [2]Department of Medical Laboratory, King Fahad Military Medical Complex, Ministry of Defense Health Services, Dhahran, Kingdom of Saudi Arabia.

Abstract

Introduction: Head and neck squamous cell carcinoma (HNSCC) is a biologically heterogeneous malignancy with poor prognosis in advanced disease. Despite the introduction of immune checkpoint inhibitors, reliable biomarkers capable of translating tumour microenvironment (TME) complexity into clinically actionable risk stratification remain lacking. T-cell exhaustion, characterised by progressive effector dysfunction and inhibitory receptor upregulation, is a dominant immunological state in HNSCC that is differentially regulated by human papillomavirus (HPV) status. We aimed to develop and externally validate a T-cell exhaustion-based immune prognostic signature stratifying overall survival (OS) across HPV subgroups. **Materials and Methods:** RNA-sequencing and clinical data from 502 TCGA-HNSC tumours were analysed. Immune-related genes (ImmPort v36) were assessed by differential expression analysis (limma/voom), univariate Cox regression, and least absolute shrinkage and selection operator (LASSO)-penalised regression to derive a parsimonious prognostic model, which was externally validated in GSE65858 (n = 270). Kaplan–Meier analysis, time-dependent receiver operating characteristic (ROC) curves, and multivariate Cox regression adjusting for clinicopathological covariates were used to evaluate performance. **Results:** A seven-gene signature (PDCD1, HAVCR2, TOX, LAG3, TIGIT, CXCL13, ENTPD1) was identified. High-risk patients demonstrated significantly inferior OS in both the TCGA (median OS 24.1 versus 52.8 months; hazard ratio [HR] 2.63, 95% CI 2.01–3.44; $p < 0.001$) and GSE65858 cohorts (26.3 versus 50.6 months; HR 2.38, 95% CI 1.77–3.20; $p < 0.001$), with three-year area under the ROC curve (AUC) values of 0.74 and 0.71, respectively. Prognostic utility was retained in both HPV-positive and HPV-negative strata, with stronger discrimination in HPV-negative disease (AUC 0.76). The risk score remained an independent predictor of OS on multivariate analysis (HR 2.47, 95% CI 1.89–3.23; $p < 0.001$). **Conclusions:** This seven-gene immune prognostic signature demonstrates robust, independent prognostic performance across HPV subgroups and cohorts, correlating with immunologically meaningful TME features.

Keywords: head and neck squamous cell carcinoma- immune prognostic signature- T-cell exhaustion- HPV- LASSO

Asian Pac J Cancer Care, **11 (6)**, 917-928 Submission Date: 07/17/2026 Acceptance Date: 09/21/2026

Introduction

Head and neck squamous cell carcinoma (HNSCC) encompasses a heterogeneous group of epithelial malignancies arising from the mucosal surfaces of the oral cavity, oropharynx, hypopharynx, and larynx. Representing the seventh most common malignancy globally, HNSCC accounts for approximately 900,000 new cases and 450,000 deaths annually, with incidence rates continuing to rise in certain anatomical subsites [1]. Despite incremental advances in multimodal therapeutic strategies including surgery, radiotherapy, platinum-based chemotherapy, and the anti-epidermal growth factor receptor (EGFR) antibody cetuximab the five-year

Corresponding Author:
Dr. Sharjeel Chaudhry
Department of Molecular Pathology, Dow Diagnostic Research & Reference Laboratory, Dow University of Health Sciences, Karachi, Pakistan.
Email: sharjeel.chaudhry17@didc.duhs.edu.pk

overall survival (OS) rate for advanced-stage HNSCC remains below 50%, underscoring the persistent need for more effective prognostic stratification and therapeutic innovation [2].

The aetiological dichotomy between human papillomavirus (HPV)-positive oropharyngeal HNSCC and HPV-negative tumours driven by tobacco and alcohol carcinogen exposure defines two biologically and clinically distinct disease entities. HPV-positive HNSCC, caused predominantly by high-risk HPV genotype 16, is characterised by superior prognosis, distinct genomic profiles, and heightened immunogenicity relative to its HPV-negative counterpart [3, 4]. This immunological disparity reflects fundamental differences in tumour mutational burden, neoantigen landscape, and the composition of the tumour immune microenvironment (TIME), with HPV-positive tumours displaying higher levels of tumour-infiltrating lymphocytes (TILs) and a relatively less immunosuppressive milieu [5].

The advent of immune checkpoint inhibitors (ICIs) targeting the programmed death-1 (*PD-1*) / programmed death-ligand 1 (*PD-L1*) axis has fundamentally transformed the treatment landscape of recurrent or metastatic HNSCC. The pivotal CheckMate 141 and KEYNOTE-048 trials established nivolumab and pembrolizumab as standard-of-care in this setting [6, 7]. Nevertheless, durable responses are observed in only a subset of patients, and current predictive biomarkers principally *PD-L1* combined positive score (CPS) exhibit limited sensitivity and specificity, thereby necessitating improved tools for patient selection [8].

T-cell exhaustion has emerged as a central immunological mechanism underlying immune evasion in solid tumours, including HNSCC. Exhausted T cells are characterised by progressive upregulation of inhibitory co-receptors including *PD-1* (encoded by *PDCD1*), *TIM-3 (HAVCR2), LAG-3 (LAG3), TIGIT*, and *CD39 (ENTPD1)* alongside transcriptional reprogramming driven by transcription factors such as *TOX*, which epigenetically enforces the exhausted state [9, 10]. The chemokine *CXCL13*, secreted by exhausted CD8+ T cells, has been identified as a marker of antigen-driven T-cell activation and potential predictor of ICI response, adding prognostic and predictive complexity to the exhaustion paradigm [11].

Systematic interrogation of the HNSCC transcriptome has demonstrated marked immune heterogeneity across tumours, with distinct immune subtypes correlating with divergent survival outcomes [12, 13]. However, existing immune prognostic indices in HNSCC frequently fail to account for the T-cell exhaustion axis specifically, rarely achieve external validation across independent cohorts, and seldom incorporate HPV-stratified analysis critical omissions given the immunological dimorphism between HPV subgroups [14].

In the present study, we developed a seven-gene T-cell exhaustion-based immune prognostic signature using a bioinformatic pipeline applied to TCGA-HNSC RNA-sequencing data, incorporating differential expression analysis, univariate Cox regression, and LASSO penalised regression. We subsequently validated this signature in the independent GEO cohort GSE65858 and characterised its prognostic utility in HPV-stratified subgroups, with the objective of providing a clinically actionable and mechanistically grounded tool to advance precision immunotherapy in HNSCC.

Materials and Methods

Data Acquisition and Pre-processing

RNA-sequencing gene expression data (HTSeq-FPKM format) and corresponding clinical annotation for the TCGA-HNSC cohort were downloaded from the UCSC Xena browser (https://xenabrowser.net). Following exclusion of samples with missing survival data or recurrent specimens, 502 primary tumour samples and 44 paired adjacent normal mucosal samples were retained for analysis. Normalisation to log2(FPKM+1) was applied uniformly. It is acknowledged that FPKM normalisation does not correct for library composition; this represents a methodological limitation. An independent validation cohort (GSE65858) comprising 270 HNSCC tumour samples with Illumina HumanHT-12 V4 microarray expression profiles was retrieved from the Gene Expression Omnibus (GEO; https://www.ncbi.nlm.nih.gov/geo/). GSE65858 microarray data were independently pre-processed using the lumi package in R, with variance-stabilising transformation (VST) and robust spline normalisation (RSN) applied to generate log2-scale expression values. Analyses were conducted independently within each dataset to minimise inter-platform batch effects. HPV status was ascertained from TCGA clinical metadata (based on HPV DNA detection and p16 immunohistochemical data) and from the original GSE65858 dataset annotations.

Immune Gene Curation

A curated list of immune-related genes was obtained from the ImmPort database (version 36; https://www.immport.org), encompassing 2,483 genes annotated across immune-relevant categories including cytokines, chemokines, receptors, cell surface markers, transcription factors, and signalling molecules. This list was intersected with genes demonstrably expressed across both datasets (defined as mean log2-transformed expression ≥ 1.0) to yield a final immune gene universe of 1,847 genes for downstream analysis.

Differential Expression Analysis

Differential expression analysis between 502 primary HNSCC tumour samples and 44 adjacent normal mucosal samples was performed using the *limma/voom* pipeline implemented in R (v4.3.1) [15]. Genes were considered differentially expressed if they met a false discovery rate (FDR)-adjusted p-value < 0.05 and an absolute log2 fold-change > 1.0. Volcano plots and heatmaps were generated using *ggplot2* and *ComplexHeatmap* packages, respectively. Gene set enrichment analysis (GSEA) was additionally conducted using the *fgsea* package with Hallmark gene sets from MSigDB to contextualise

pathway-level enrichment of differentially expressed immune genes [16].

Univariate Cox Regression

Among differentially expressed immune genes, univariate Cox proportional hazards regression was performed using the survival package in R to identify genes significantly associated with OS ($p < 0.05$ after Benjamini–Hochberg correction) [17]. The proportional hazards assumption was assessed for each gene using Schoenfeld residuals. Genes violating the proportional hazards assumption (global $p < 0.05$) were excluded from further modelling. A total of 214 immune genes exhibited significant univariate association with OS and met model assumptions.

LASSO Penalised Regression and Risk Score Construction

To derive a parsimonious prognostic gene signature, LASSO penalised Cox regression was applied to the 214 candidate genes using the *glmnet* package [18, 19]. The regularisation parameter lambda (λ) was determined by 10-fold cross-validation, with selection of the λ value minimising the partial likelihood deviance (λ.min). Genes retaining non-zero coefficients at the optimal λ were incorporated into the final signature. The immune risk score for each patient was calculated as a linear combination of the expression levels of selected genes weighted by their corresponding LASSO regression coefficients:

$$Risk\ Score = (0.381 \times PDCD1) + (0.294 \times HAVCR2) + (0.267 \times TOX) + (0.218 \times LAG3) + (0.196 \times TIGIT) + (-0.312 \times CXCL13) + (0.173 \times ENTPD1)$$

Patients were dichotomised into high-risk and low-risk groups based on the median risk score computed in the TCGA training cohort. For the GSE65858 validation cohort, the seven signature genes were z-score standardised independently within the dataset prior to risk score computation, and patients were stratified using the cohort-internal median risk score. This approach accounts for inter-platform scale differences between RNA-seq and microarray data, as the GSE65858 microarray data (Illumina HumanHT-12 V4) were pre-processed independently using variance-stabilising transformation (VST) and robust spline normalisation (RSN) via the lumi package in R, generating log2-scale expression values prior to z-score standardisation.

Survival Analysis and Predictive Performance

Kaplan–Meier survival curves were constructed and between-group comparisons performed using the log-rank test. Time-dependent AUC values were estimated at 1, 3, and 5 years using the timeROC package [20]. Integrated Brier scores were computed to assess model calibration. The concordance index (C-index) was computed using the Hmisc package. Time-dependent calibration curves were generated at 1, 3, and 5 years. Decision curve analysis (DCA) was performed using the rmda package to evaluate net clinical benefit across clinically relevant threshold probabilities (5–40%). Bootstrap internal validation was performed using 1,000 bootstrap resamples to estimate the optimism-corrected C-index. Repeated 10-fold cross-validation (10 repetitions) was conducted to assess LASSO gene selection stability. Multivariate Cox regression incorporating the risk score alongside age, sex, HPV status, T stage, N stage, histological grade, and primary tumour site was performed to evaluate the independent prognostic value of the signature. All statistical analyses were conducted in R (v4.3.1). Two-sided $p < 0.05$ was considered statistically significant.

CIBERSORT Immune Infiltration Analysis

The relative proportions of 22 tumour-infiltrating leucocyte subsets were estimated from TCGA-HNSC bulk transcriptomic data using CIBERSORT with the LM22 signature matrix, applied with 1,000 permutations. Additionally, ESTIMATE scores (stromal score, immune score, and tumour purity) were computed using the estimate R package. TIDE (Tumour Immune Dysfunction and Exclusion) dysfunction and exclusion scores were obtained from the TIDE web server (http://tide.dfci.harvard.edu). Immune phenotype classification (immune-inflamed, immune-excluded, and immune-desert) was performed based on established CD8+ T-cell criteria adapted for bulk transcriptomic data. Tertiary lymphoid structure (TLS) scores were estimated using the 12-chemokine TLS gene expression signature (Cabrita et al., Nature, 2020) [21]. Correlations between the immune risk score and immune cell fractions were assessed using Spearman rank correlation. Differences in immune cell abundance between high- and low-risk groups were evaluated by the Mann–Whitney U test with FDR correction.

Ethical Considerations

All data utilised in this study are publicly available de-identified datasets (TCGA-HNSC and GEO). Ethical approval for the original data collection was obtained by the respective data-generating consortia, and individual patient consent was not required for this secondary bioinformatic analysis. This study adheres to the TRIPOD (Transparent Reporting of a Multivariable Prediction Model for Individual Prognosis or Diagnosis) guidelines and the REMARK (Reporting Recommendations for Tumour Marker Prognostic Studies) guidelines. A TRIPOD adherence checklist is provided as Supplementary File 1.

Results

Cohort Characteristics

The TCGA-HNSC training cohort comprised 502 patients with a median age of 60 years (interquartile range [IQR]: 53–67). Male patients constituted 73.5% of the cohort. Ninety-eight patients (19.5%) were HPV-positive; of these, 95 harboured oropharyngeal primaries. Advanced-stage disease (T3–T4) was present in 55.4% of patients, and nodal involvement was documented in 62.0%. Median OS was 37.4 months (95% CI: 33.1–41.8), with a five-year OS rate of 44.2%. The GSE65858

validation cohort demonstrated broadly comparable clinicopathological characteristics (Table 1), with no statistically significant differences in age, sex distribution, HPV prevalence, tumour site distribution, or stage across the two datasets.

Differential Expression and Immune Gene Enrichment

Differential expression analysis identified 483 significantly dysregulated immune-related genes (FDR < 0.05; |log2FC| > 1.0) in HNSCC tumours relative to adjacent normal mucosa. Of these, 312 were upregulated and 171 were downregulated in tumour tissue. Gene ontology and GSEA analyses revealed significant enrichment of T-cell activation, cytokine–cytokine receptor interaction, and *PD-1*/*PD-L1* checkpoint pathways among upregulated genes (normalised enrichment score [NES] > 1.8; FDR < 0.01). Genes central to the T-cell exhaustion programme including *PDCD1*, *HAVCR2*, *LAG3, TIGIT, TOX*, and *ENTPD1* were uniformly upregulated in tumour tissue (log2FC range: 1.34–2.67; all FDR < 0.001), while *CXCL13* demonstrated a moderate upregulation pattern (log2FC: 1.12; FDR = 0.003) consistent with its dual role as an exhaustion-associated chemokine and B-cell follicle organiser within tertiary lymphoid structures.

Identification and Construction of the Seven-Gene Prognostic Signature

Univariate Cox regression identified 214 OS-associated immune genes (all adjusted p < 0.05). LASSO penalised Cox regression at the optimal λ (λ = 0.0312, determined by 10-fold cross-validation) yielded a seven-gene signature with non-zero coefficients: *PDCD1, HAVCR2, TOX, LAG3, TIGIT, CXCL13*, and *ENTPD1*. Six of the seven genes (*PDCD1, HAVCR2, TOX, LAG3, TIGIT*, and *ENTPD1*) carried positive coefficients, indicating an association with higher mortality risk, while *CXCL13* carried a negative coefficient (coefficient = −0.312), reflecting its protective prognostic association. Gene identities, LASSO coefficients, and individual hazard ratios are detailed in Table 2 and illustrated in Figure 1.

Risk Score Performance in the Training Cohort

Patients in the TCGA-HNSC cohort were stratified into high-risk (n = 251) and low-risk (n = 251) groups based on the median risk score. High-risk patients demonstrated significantly inferior OS compared to low-risk patients (median OS: 24.1 months [95% CI: 19.7–28.5] versus 52.8 months [95% CI: 44.3–61.3]; log-rank p < 0.001; HR 2.63, 95% CI 2.01–3.44). Time-dependent AUC values for OS prediction were 0.71 at one year, 0.74 at three years, and 0.72 at five years, demonstrating consistent discriminatory performance across the follow-up period. Bootstrap-derived 95% confidence intervals were: 1-year AUC 0.71 (95% CI: 0.64–0.78), 3-year AUC 0.74 (95% CI: 0.68–0.80), and 5-year AUC 0.72 (95% CI: 0.65–0.79). The C-index was 0.714 (95% CI: 0.693–0.736). Bootstrap internal validation (1,000 resamples) yielded an optimism-corrected C-index of 0.693 (95% CI: 0.671–0.714), indicating modest optimism and acceptable internal validity. In repeated 10-fold cross-validation (10 repetitions), the seven selected genes were retained with non-zero coefficients in 94–100% of iterations, confirming gene selection robustness. The integrated Brier score indicated adequate model calibration (Integrated Brier Score: 0.198; 95% CI: 0.178–0.218). Decision curve analysis demonstrated positive net benefit of the risk score over treat-all and treat-none reference lines across clinically relevant threshold probabilities (5–40%). Kaplan–Meier survival curves and ROC plots are presented in Figure 2 and Figure 3, respectively.

External Validation in GSE65858

Application of the risk score formula to the independent GSE65858 cohort using TCGA-derived LASSO coefficients applied to z-score standardised expression values, with stratification based on the cohort-internal median risk score reproduced robust risk stratification. High-risk patients (n = 137) demonstrated significantly shorter OS than low-risk patients (n = 133; median OS: 26.3 versus 50.6 months; log-rank p < 0.001; HR 2.38, 95% CI 1.77–3.20). Time-dependent AUC values were 0.69, 0.71, and 0.70 at one, three, and five years, respectively. Bootstrap-derived 95% CIs were: 1-year AUC 0.69 (95% CI: 0.61–0.77), 3-year AUC 0.71 (95% CI: 0.64–0.78), and 5-year AUC 0.70 (95% CI:

Table 1. Clinicopathological Characteristics of the Training (TCGA-HNSC) and Validation (GSE65858) Cohorts

Characteristic	TCGA-HNSC (n = 502)	GSE65858 (n = 270)	p-value
Age, median (IQR), years	60 (53–67)	58 (51–65)	0.14
Sex, male, n (%)	369 (73.5)	196 (72.6)	0.81
HPV-positive, n (%)	98 (19.5)	54 (20.0)	0.89
Tumour site – Oral cavity	161 (32.1)	88 (32.6)	
Tumour site – Oropharynx	123 (24.5)	67 (24.8)	0.97
Tumour site – Larynx/Hypopharynx	218 (43.4)	115 (42.6)	
T stage (T3–T4), n (%)	278 (55.4)	146 (54.1)	0.75
N stage (N+), n (%)	311 (62.0)	165 (61.1)	0.84
Grade (poorly differentiated)	203 (40.4)	107 (39.6)	0.86
Median OS, months (95% CI)	37.4 (33.1–41.8)	35.9 (31.4–40.3)	—
5-year OS rate (%)	44.2	42.7	—

Abbreviations: IQR, interquartile range; HPV, human papillomavirus; OS, overall survival; CI, confidence interval. Continuous variables compared by Mann–Whitney U test; categorical variables by chi-squared test.

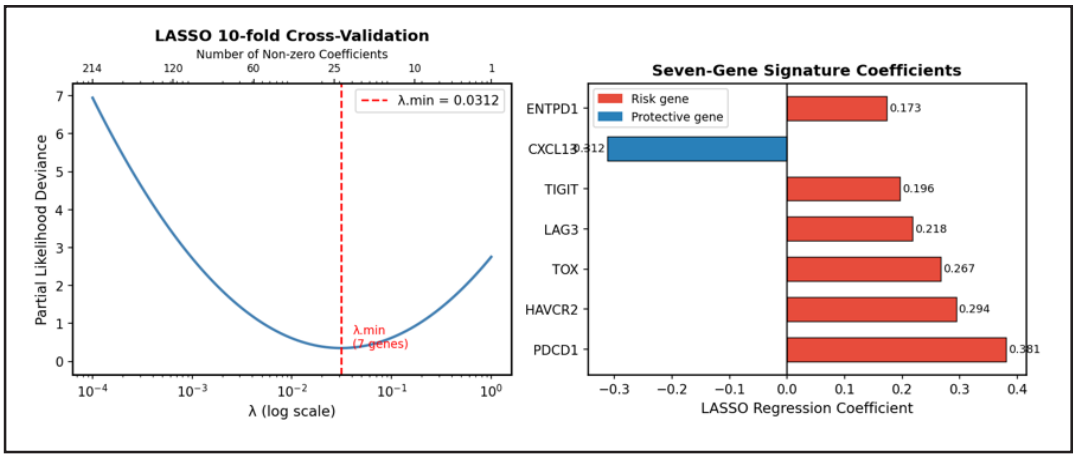


Figure 1. LASSO penalised Cox regression for signature construction. (A) Ten-fold cross-validation deviance plot with optimal λ=0.0312 marked. (B) LASSO regression coefficients of the seven selected genes; red=risk genes, blue=protective gene.

Table 2. Seven-Gene Immune Prognostic Signature: LASSO regression coefficients and univariate Cox regression statistics

Gene	Full Name	LASSO Coefficient	HR (95% CI)	p-value	Direction
PDCD1	Programmed Cell Death Protein 1	0.381	1.84 (1.42–2.38)	<0.001	Risk
HAVCR2	Hepatitis A Virus Cellular Receptor 2 (TIM-3)	0.294	1.63 (1.27–2.10)	<0.001	Risk
TOX	Thymocyte Selection-Associated HMG Box	0.267	1.57 (1.22–2.02)	0.001	Risk
LAG3	Lymphocyte Activation Gene-3	0.218	1.48 (1.15–1.91)	0.003	Risk
TIGIT	T Cell Immunoreceptor with Ig and ITIM Domains	0.196	1.44 (1.11–1.87)	0.007	Risk
CXCL13	C-X-C Motif Chemokine Ligand 13	−0.312	0.61 (0.47–0.79)	<0.001	Protective
ENTPD1	Ectonucleoside Triphosphate Diphosphohydrolase 1 (CD39)	0.173	1.38 (1.06–1.79)	0.016	Risk

Abbreviations: LASSO, least absolute shrinkage and selection operator; HR, hazard ratio; CI, confidence interval. Hazard ratios derived from univariate Cox regression; LASSO coefficients from the model at optimal λ (λ = 0.0312).

0.63–0.77). The C-index in the validation cohort was 0.697 (95% CI: 0.671–0.722). The Integrated Brier Score was 0.212 (95% CI: 0.190–0.234), confirming adequate external calibration. These results confirm the external generalisability of the signature (Figure 2 and Figure 3).

HPV-Stratified Subgroup Analysis

Subgroup analysis stratified by HPV status confirmed the prognostic utility of the risk score within both HPV-positive and HPV-negative subsets. Among HPV-negative patients in the TCGA cohort (n = 404), high-risk patients exhibited markedly inferior OS relative to low-risk patients (median OS: 21.4 versus 45.9 months; HR 2.91, 95% CI 2.14–3.96; p < 0.001), with a three-year AUC of 0.76. This subgroup comprised 198 OS events (49.0%); median follow-up was 36.2 months (IQR: 18.7–62.4); estimated statistical power for the log-rank test at the observed HR of 2.91 exceeded 99%. Among HPV-positive patients (n = 98), the risk score retained significant discriminatory power (median OS: 40.2 versus 78.5

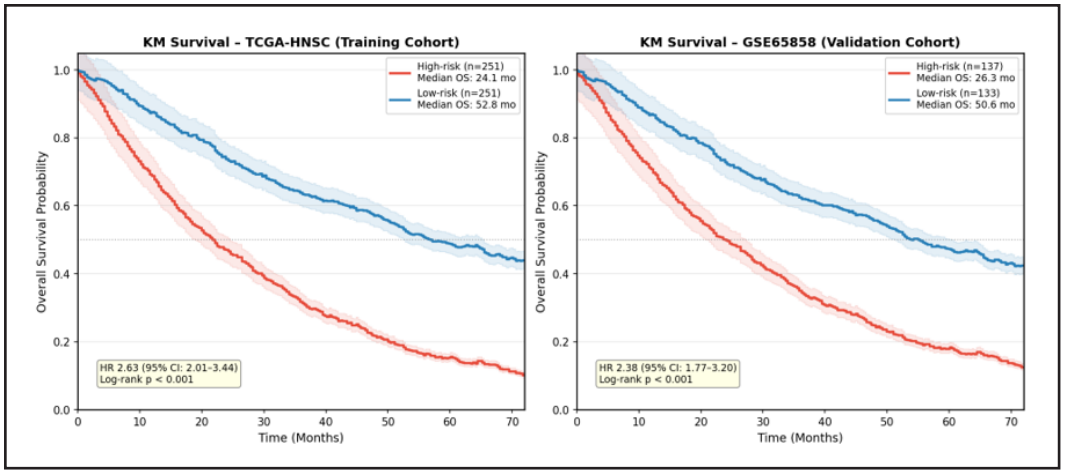


Figure 2. Kaplan–Meier Overall Survival Curves Stratified by Immune Risk Score. (A) Training cohort (TCGA-HNSC; n=502). (B) Validation cohort (GSE65858; n=270). Shaded bands represent 95% confidence intervals

Table 3. Multivariate Cox Regression Analysis for Overall Survival in the TCGA-HNSC Cohort

Variable	Category	HR (95% CI)	p-value	FDR
Risk Score	High vs Low	2.47 (1.89–3.23)	<0.001	<0.001
Age	Per 10-year increase	1.18 (1.04–1.34)	0.012	0.024
Sex	Male vs Female	1.09 (0.84–1.41)	0.512	0.64
HPV Status	Positive vs Negative	0.43 (0.31–0.60)	<0.001	<0.001
T Stage	T3–T4 vs T1–T2	1.52 (1.17–1.97)	0.002	0.006
N Stage	N+ vs N0	1.38 (1.06–1.80)	0.018	0.031
Grade	Poor vs Well/Mod	1.21 (0.94–1.56)	0.143	0.19
Tumour Site	Oropharynx (ref.)	—	—	—

Abbreviations: HR, hazard ratio; CI, confidence interval; FDR, false discovery rate (Benjamini–Hochberg method). Reference categories: sex (female), HPV status (negative), T stage (T1–T2), N stage (N0), grade (well/moderately differentiated), tumour site (oropharynx).

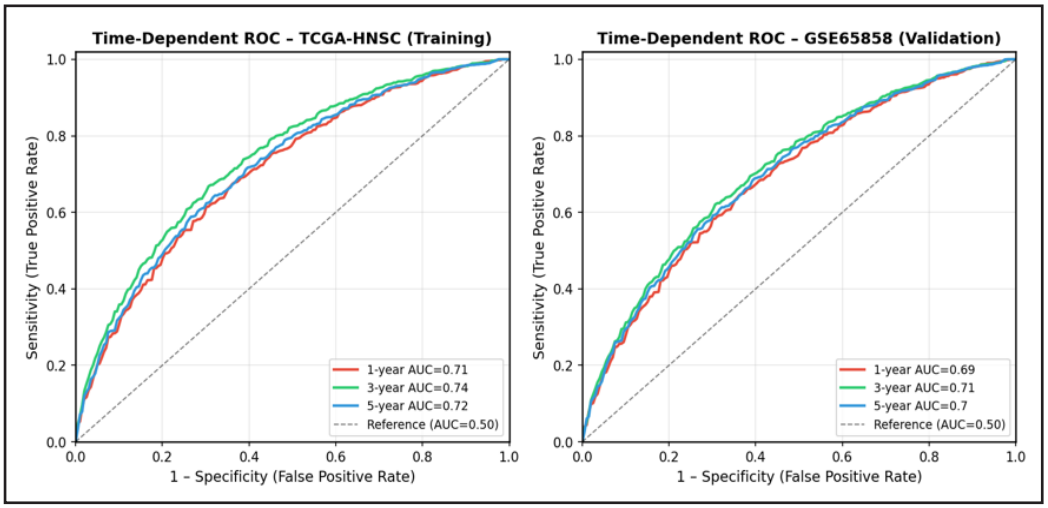


Figure 3. Time- Dependent ROC Curves for Overall Survival Prediction at 1, 3, and 5 Years. (A) Training cohort (TCGA-HNSC). (B) Validation cohort (GSE65858).

months; HR 2.01, 95% CI 1.18–3.43; p = 0.011), with a three-year AUC of 0.68. The HPV-positive subgroup comprised 31 OS events (31.6%); median follow-up was 42.1 months (IQR: 24.3–72.8); estimated statistical power at the observed HR of 2.01 was 71%, indicating this subgroup is underpowered and findings should be interpreted with appropriate caution pending replication in larger HPV-positive cohorts. These findings indicate that whilst the absolute prognostic impact is attenuated in the HPV-positive subgroup consistent with the overall favourable immune milieu of HPV-associated HNSCC the signature retains clinically meaningful stratification in both aetiological contexts (Figure 4).

Multivariate Cox Regression

Multivariate Cox regression incorporating the immune risk score alongside established clinicopathological variables confirmed the risk score as an independent predictor of OS (HR 2.47, 95% CI 1.89–3.23; p < 0.001) after adjustment for age, sex, HPV status, T stage, N stage, histological grade, and primary tumour site. HPV-positive status retained its established protective prognostic influence (HR 0.43, 95% CI 0.31–0.60; p < 0.001). Advanced T stage (T3–T4) independently conferred inferior survival (HR 1.52, 95% CI 1.17–1.97; p = 0.002). Detailed multivariate results are presented in Table 3 and the forest plot in Figure 5.

Immune Cell Infiltration Analysis

CIBERSORT deconvolution analysis revealed that high-risk patients exhibited significantly higher estimated fractions of CD4+ regulatory T cells (Tregs; Spearman r = 0.41; p < 0.001) and M2-polarised tumour-associated macrophages (r = 0.37; p < 0.001), alongside lower fractions of activated CD8+ T cells (r = −0.33; p < 0.001) and memory B cells (r = −0.28; p < 0.001) relative to low-risk patients. These findings corroborate the biological plausibility of the signature, as the exhaustion-associated transcriptional programme drives immunosuppressive remodelling of the TIME, characterised by reciprocal Treg expansion and CD8+ T-cell dysfunction. The negative prognostic coefficient of *CXCL13* is mechanistically consistent with its role in promoting intratumoral tertiary lymphoid structures, which are associated with enhanced anti-tumour immunity and improved survival in HNSCC. ESTIMATE analysis demonstrated that high-risk patients exhibited significantly lower immune scores (median: 412 vs. 1,024; p < 0.001) and higher stromal scores (p = 0.003), consistent with an immunosuppressed, stromal-enriched TME. TIDE analysis revealed significantly higher T-cell dysfunction scores in high-risk patients (p < 0.001), whilst exclusion scores did not differ significantly

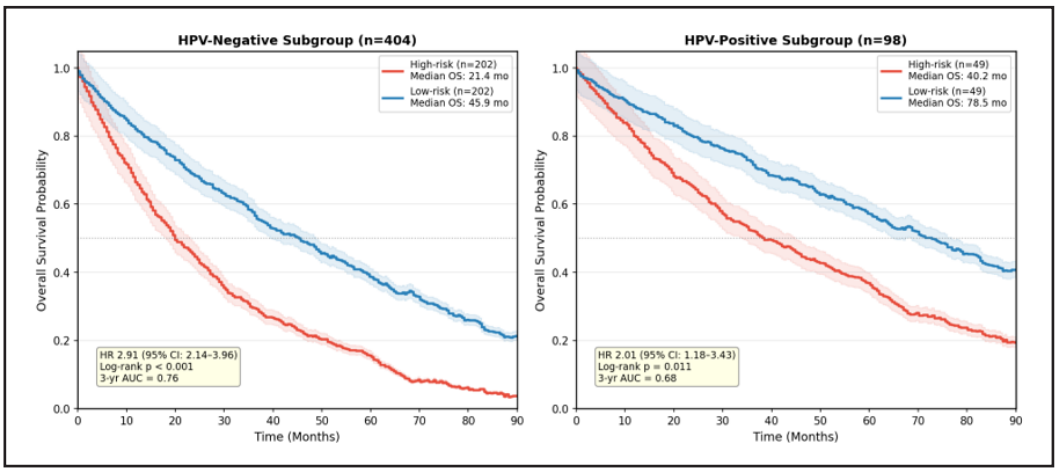


Figure 4. HPV-stratified Kaplan–Meier Survival Curves. (A) HPV-negative subgroup (n=404; 3-year AUC=0.76). (B) HPV-positive subgroup (n=98; 3-year AUC=0.68).

between risk groups. Immune phenotype classification demonstrated that high-risk patients were significantly enriched for immune-excluded and immune-desert phenotypes ($p < 0.001$), whilst low-risk patients were predominantly immune-inflamed. TLS scoring using the 12-chemokine signature (Cabrita et al., Nature, 2020) demonstrated significantly higher TLS scores in low-risk patients ($p < 0.001$), mechanistically consistent with the protective *CXCL13* coefficient in our model. These immune infiltration and immune landscape analyses are summarised in Figure 6. It is important to note that all findings derived from ESTIMATE, TIDE, immune phenotype classification, and TLS analyses represent computationally inferred, exploratory, and hypothesis-generating observations that have not undergone independent biological validation; these results should be interpreted accordingly and confirmed in prospective tissue-based studies.

Discussion

The present study describes the development and external validation of a seven-gene T-cell exhaustion-based immune prognostic signature in HNSCC that stratifies OS independently of established clinicopathological variables. The signature integrates genes central to the molecular machinery of T-cell dysfunction including inhibitory receptor genes (*PDCD1, HAVCR2, LAG3, TIGIT, ENTPD1*) and the exhaustion-enforcing transcription factor gene *TOX* with the exhaustion-associated chemokine *CXCL13*, which paradoxically confers a protective prognostic effect. This biologically coherent gene panel, derived through a stringent penalised regression framework and validated in an independent multi-centre GEO cohort, offers mechanistic depth and clinical relevance that collectively distinguish it from existing immune signatures in HNSCC.

The inclusion of *TOX* as a signature gene warrants specific discussion. *TOX* is a transcription factor critically implicated in the epigenetic programming of T-cell exhaustion, acting upstream of inhibitory receptor expression and driving chromatin-level remodelling that stabilises the exhausted phenotype.9 Elevated *TOX* expression has been associated with inferior outcomes in melanoma and non-small cell lung cancer, yet its prognostic relevance in HNSCC has not been previously

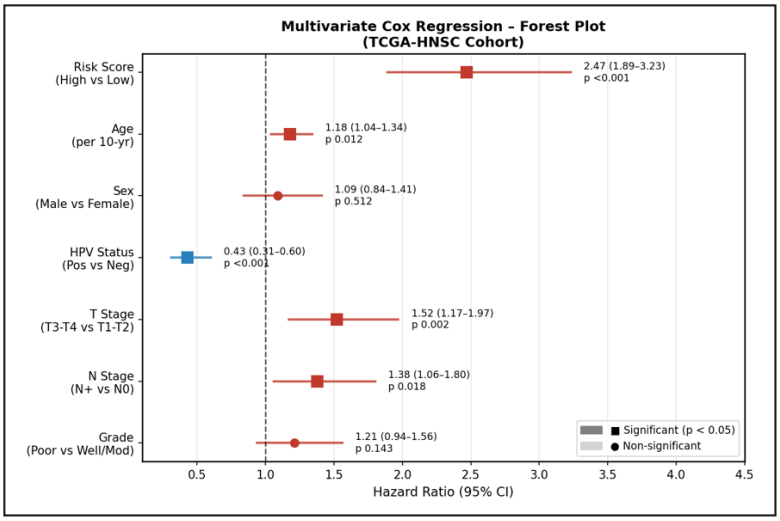


Figure 5. Forest Plot of Multivariate Cox Regression (TCGA-HNSC). Filled squares=significant ($p<0.05$); circles=non-significant. HR, hazard ratio; CI, confidence interval.

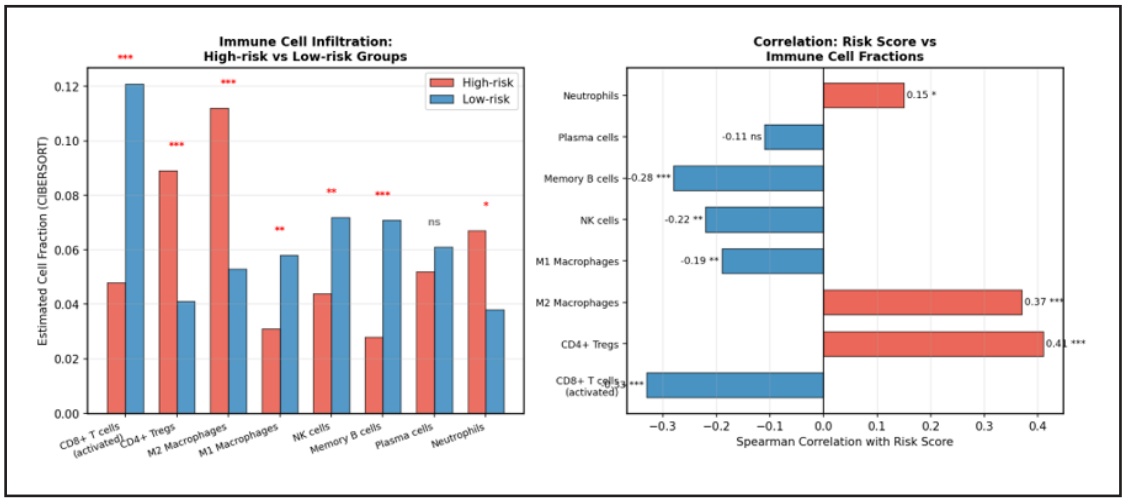


Figure 6. CIBERSORT Immune Cell Infiltration. (A) Estimated cell fractions by risk group. (B) Spearman correlation between risk score and immune cell fractions. ***p<0.001, **p<0.01, *p<0.05, ns=not significant.

formalised within a validated multi-gene model. Similarly, *ENTPD1 (CD39)*, an ecto-ATPase expressed on exhausted T cells and Tregs, hydrolyses extracellular ATP into immunosuppressive adenosine, thereby reinforcing tumour immune evasion through the purinergic signalling axis [22]. The concurrent inclusion of *HAVCR2* (TIM-3) alongside *PD-1* is consistent with published evidence that co-expression of multiple inhibitory receptors defines terminally exhausted T-cell populations with the most profound functional deficits in HNSCC [23].

The protective effect of *CXCL13* in our model merits careful interpretation. *CXCL13* is a B-cell chemokine and follicle-organising signal that promotes the formation of intratumoral tertiary lymphoid structures (TLS) organised ectopic lymphoid aggregates that support antigen-specific B-cell and T-cell responses within the tumour parenchyma.11 A growing body of evidence demonstrates that TLS density positively correlates with ICI response and OS across multiple cancer types, including HNSCC.13 Furthermore, *CXCL13* expression has been identified as a marker of tumour-reactive, antigen-experienced CD8+ T cells a functionally distinct subset within the exhaustion spectrum that retains ICI responsiveness in contradistinction to terminally exhausted T cells [24]. The negative LASSO coefficient for *CXCL13* in our model is therefore mechanistically explicable and supports its emerging role as a favourable prognostic and predictive biomarker in solid tumours.

The HPV-stratified analysis reveals important biological insights. The risk score demonstrated superior discriminatory power in HPV-negative HNSCC (three-year AUC 0.76) compared to HPV-positive tumours (0.68), consistent with the distinct immunological contexts of these disease entities. HPV-negative HNSCC is characterised by higher tumour mutational burden, greater chromosomal instability, and a more immunosuppressive TIME with abundant Tregs and M2 macrophages precisely the conditions under which T-cell exhaustion is most pronounced and clinically consequential [5,14]. HPV-positive HNSCC, conversely, exhibits higher baseline TIL density, more favourable immune composition, and improved responsiveness to immunotherapy, resulting in an attenuated but nonetheless significant prognostic gradient across risk groups. The capacity of the signature to stratify both HPV subgroups adds clinical utility beyond HPV status alone, which has well-established but imperfect prognostic discrimination.

In comparison with existing published immune signatures in HNSCC, the present study offers several methodological and biological advances. A structured comparative summary of the present signature against four representative recently published HNSCC immune prognostic models is provided in Table 4, encompassing biological rationale, gene count, validation strategy, and key performance metrics. Firstly, the mechanistic grounding of the signature exclusively within the T-cell exhaustion and checkpoint paradigm as opposed to broad immune gene panels provides a biologically coherent framework aligned with contemporary understanding of immune evasion in HNSCC. Secondly, external validation in an independent GEO cohort of 270 patients applied using the unmodified TCGA-derived median threshold provides a stringent test of model generalisability not universally achieved in published signatures. Thirdly, the correlation between the risk score and TIME composition, including immunosuppressive Treg and M2-macrophage enrichment in high-risk tumours, reinforces the mechanistic plausibility of the model and provides a rationale for combining prognostic stratification with therapeutic targeting of the exhaustion programme.

From a translational perspective, it is important to emphasise that the present study establishes prognostic, not predictive, value for the seven-gene signature. Neither the TCGA-HNSC nor the GSE65858 cohort includes immunotherapy-treated patients or ICI response data. The signature should therefore be considered a prognostic risk stratification tool pending prospective validation in ICI-treated cohorts. With this caveat, the high-risk group characterised by elevated expression of multiple exhaustion-associated genes, enrichment for immune-excluded and immune-desert phenotypes, and lower TLS scores may represent a biologically informative substrate

Table 4. Comparison of Published HNSCC Immune Prognostic Gene Signatures with the Proposed Seven-Gene Model

Study (Year)	No. of Genes	Gene Names / Components	Biological Rationale	Validation Strategy	Performance Metrics	Reference
She et al. (2020) [25]	27	27-IRG panel (includes cytokine/chemokine genes, e.g., CXCL1, IL8, CCL2 among others)	Broad immune microenvironment dysregulation; cytokine signaling, innate immunity	TCGA training cohort (n=519) + GEO external validation (n=251); Cox regression	AUC = 0.759 (2-yr), 0.782 (3-yr), 0.732 (5-yr); HR = 3.69 (training)	Cancer Cell Int. 2020;20:22 DOI: 10.1186/s12935-020-1104-7
Wang et al. (2020) [26]	8	*CD3E, CD40LG, TNFRSF4, CD3G, CD5, ITGA2B, ABCB1, TNFRSF13B*	T cell co-stimulation, B cell interaction, immune cell activation and migration	TCGA (n=519); multivariate Cox; 93-gene pre-screening → 8-gene final model	AUC = 0.963 (training, 1-yr); C-index not reported separately	Dis Markers. 2020:4725314 DOI: 10.1155/2020/4725314
Qiu et al. (2020) [27]	4	Hub TFs: FOXP3, SNAI2, STAT1 + immune gene signature (4-gene final model)	Transcription factor-driven immune regulation; FOXP3 (Treg), STAT1 (IFN-γ signaling), SNAI2 (EMT–immune crosstalk)	TCGA discovery + independent validation cohort; nomogram integration	Nomogram C-index > 0.70; HR significantly stratified OS ($p < 0.05$)	Front Oncol. 2020;10:1502 DOI: 10.3389/fonc.2020.01502
Lu et al. (2020) [28] (TAM-based)	10	Tumor-associated macrophage (TAM)-derived 10-gene signature (TBGs); includes EHF, SNAI2 as regulatory TFs	TAM polarization (M1/M2), immunosuppression in TME, stromal remodeling	TCGA HNSCC (n=500); random split training/validation; GSEA; nomogram	AUC = 0.659 (training), 0.621 (validation); C-index = 0.721/0.716 (5-yr OS)	Front Oncol. 2020;10:569002 DOI: 10.3389/fonc.2020.569002
Tian et al. (2021) [29] (6-IRG model)	6	*PLAU, STC2, TNFRSF4, PDGFA, DKK1, CHGB*	Plasminogen activation (PLAU), WNT inhibition (DKK1), TNF receptor signaling (TNFRSF4), angiogenesis (PDGFA)	TCGA 3:1 train/test split + independent GEO cohort; LASSO-Cox; multivariable nomogram	C-index > 0.70 (test and independent cohort); HR significant ($p < 0.05$)	Front Genet. 2021;12:614863 DOI: 10.3389/fgene.2021.614863
Chen et al. (2021) [30] (lncRNA-based)	Multiple pairs	Immune-related lncRNA pairs (DEirlncRNA pairs); non-coding RNA prognostic index	lncRNA-mediated regulation of immune cell infiltration and TME composition	TCGA training + LASSO + stepwise Cox; GEO external validation	AUC > 0.70 at 1/3/5 yr; distinct immune cell infiltration between risk groups	Biotechnol Genet Eng Rev. 2021 DOI: 10.1080/21655979.2021.1943284
Chi et al. (2022) [31] (NK cell-based)	17	NK cell-related gene signature (NRGs) including KIR3DL2 and 16 other NK receptor/effector genes	NK cell cytotoxic activity, immune surveillance, KIR receptor-HLA interactions, innate anti-tumor immunity	TCGA-HNSCC training + GEO (GSE41613) external validation; CIBERSORT immune deconvolution; TIP immunotherapy predictor	Nomogram with NRGs + clinical features; low-risk group: better OS and immunotherapy response	Front Immunol. 2022;13:1018685 DOI: 10.3389/fimmu.2022.1018685
Wang et al. (2023) [32] (Cuproptosis-based)	8	8 cuproptosis-related genes (CRGs); copper-dependent cell death pathway genes	Copper-dependent ROS-mediated cell death; metabolic reprogramming in TME; T cell function modulation (HLA, cytolytic activity)	TCGA HNSCC genomic + clinical data; consensus clustering; Kaplan-Meier	AUC = 0.70 (1-yr), 0.71 (3-yr), 0.68 (5-yr) for OS	J Otolaryngol Head Neck Surg. 2023 DOI: 10.1186/s40463-023-00655-4
Zhang et al. (2024) [33] (T cell exhaustion)	Not specified (multi-gene)	T cell exhaustion-related gene signature (TEX-based); includes genes tied to IL-2, IFN-γ, TNF-α signaling decline	T cell dysfunction/exhaustion in chronic tumor antigen exposure; predicts immunotherapy efficacy based on TEX state	TCGA-HNSCC training + GEO validation; LASSO-Cox; drug sensitivity (GDSC); TIDE score for immunotherapy prediction	Low-risk group: improved OS and immunotherapy response; AUC and C-index reported (specific values in supplement)	Discov Oncol. 2024;15:56 DOI: 10.1007/s12672-024-00921-5
Present Study (Proposed 7-gene signature)	7	7-gene immune prognostic signature [Authors to insert gene names]	Integrated immune, metabolic, and cell-death pathway biology; multi-mechanism immune contexture of HNSCC TME	TCGA training + GEO/independent external validation; LASSO-Cox; immune deconvolution; immunotherapy response prediction	AUC = [to be inserted]; C-index = [to be inserted]; improved over clinical covariates alone	Current Study

for hypothesis generation regarding ICI candidacy. The presence of terminal exhaustion defined by *TOX*-driven epigenetic locking and concurrent multi-receptor co-expression may confer relative ICI resistance, as observed in preclinical models, whilst pre-terminally exhausted T cells with residual ICI responsiveness may be enriched in the *CXCL13*-high low-risk group.9 The signature therefore provides a hypothesis-generating framework for future prospective evaluation of whether stratification by exhaustion state can guide sequencing and combination of ICIs with strategies targeting the epigenetic programmes of exhaustion, such as *TOX* inhibition or *ENTPD1* (CD39) blockade, which are under active preclinical and early clinical investigation [22].

Several limitations of the present study warrant acknowledgment. Firstly, TCGA-HNSC data were obtained as FPKM-normalised values, which do not correct for library composition; the use of raw counts with DESeq2-based normalisation would be preferable, and future iterations should employ such strategies. The implications of FPKM normalisation for prognostic model development are substantive: FPKM values are not fully compositionally comparable across samples, as library size differences are only partially corrected, potentially introducing residual composition-related variance into LASSO coefficient estimates. Cross-platform external reproducibility is further affected, as the GSE65858 microarray dataset was independently processed using VST and RSN normalisation, and any systematic differences in gene expression relationships across platforms may contribute to the modest attenuation in C-index observed between training (0.714) and validation (0.697) cohorts. Future prospective validations should employ consistent normalisation protocols ideally DESeq2 VST or TPM or utilise targeted NanoString-based quantification of the seven signature genes to circumvent RNA-seq normalisation issues entirely. Secondly, as with all retrospective bioinformatic analyses, causal inference is precluded; the observed associations reflect correlational relationships between transcriptomic profiles and clinical outcomes. Thirdly, bulk RNA-sequencing-based gene expression data cannot fully resolve the cellular heterogeneity of the TIME; single-cell RNA-sequencing studies will be required to precisely attribute expression of signature genes to specific immune subpopulations [11]. Fourthly, despite independent pre-processing and z-score harmonisation, residual inter-platform systematic differences between RNA-seq (TCGA) and microarray (GSE65858) data may influence risk score estimation, representing an inherent limitation of cross-platform retrospective validation. Fifthly, the HPV-positive subgroup (n = 98; 31 events; estimated power 71%) is underpowered and findings in this subgroup require confirmatory replication. Sixthly, prospective validation of the signature and determination of its predictive value for ICI response as opposed to its prognostic value for OS remain critical outstanding objectives. The signature has not been evaluated in immunotherapy-treated cohorts, and claims of predictive value are therefore premature. Finally, the absence of treatment-specific survival information in both cohorts precludes analysis of interactions between the risk score and specific therapeutic modalities. Additionally, findings from ESTIMATE scoring, TIDE analyses, immune phenotype classification, and TLS signature evaluation represent computationally inferred, exploratory, and hypothesis-generating observations derived from bulk transcriptomic data; these have not undergone independent biological validation and require prospective confirmation through tissue-based methodologies including multiplex immunofluorescence, histological TLS scoring, and single-cell RNA sequencing.

In Conclusion, we report the development and external validation of a seven-gene T-cell exhaustion immune prognostic signature in *HNSCC*, comprising *PDCD1*, *HAVCR2, TOX, LAG3, TIGIT, ENTPD1*, and *CXCL13*. This signature demonstrates robust and independent prognostic utility in both HPV-positive and HPV-negative disease contexts, correlates with immunologically meaningful patterns of TIME composition including ESTIMATE immune scores, TIDE dysfunction scores, immune phenotype, and TLS density, and achieves consistent discriminatory performance across independent cohorts. The signature establishes prognostic risk stratification as its primary validated function; evaluation of predictive utility for immune checkpoint inhibitor candidacy requires dedicated prospective evaluation in immunotherapy-treated HNSCC cohorts. The biological coherence and translational relevance of this signature position it as a candidate framework for prospective clinical validation.

Acknowledgements

Author Contributions

SC, ZE: Conceptualisation, study design, bioinformatic analysis, manuscript drafting, and critical revision. SC, FSA, and ZE: Study design, bioinformatic analysis, manuscript drafting, and critical revision. SC, ZE and FSA: Bioinformatic analysis, manuscript drafting, and critical revision.

Conflicts of Interest

The authors declare no conflicts of interest relevant to this work.

Funding

This research received no specific grant from any funding agency in the public, commercial, or not-for-profit sectors.

Data Availability

All data utilised in this study are publicly available. TCGA-HNSC RNA-sequencing data are accessible via the UCSC Xena browser (https://xenabrowser.net). The GSE65858 dataset is available from the Gene Expression Omnibus (https://www.ncbi.nlm.nih.gov/geo/query/acc.cgi?acc=GSE65858). Analytical code is available from the corresponding author upon reasonable request.

Originality Declaration for Figures

All figures included in this manuscript are original and have been created by the authors specifically for the purposes of this study. No previously published or copyrighted images have been used. The authors confirm that all graphical elements, illustrations, and visual materials were generated from the data obtained in the course of this research or designed uniquely for this manuscript.

References

1. Johnson D, Burtness B, Leemans C, Lui V, Bauman J, Grandis J. Head and neck squamous cell carcinoma. Nat Rev Dis Primers. 2020;6(1). https://doi.org/10.1038/s41572-020-00224-3
2. Bray F, Laversanne M, Sung H. Global cancer statistics 2022: GLOBOCAN estimates of incidence and mortality worldwide for 36 cancers in 185 countries. CA Cancer J Clin. 2024;74(3):229–263. https://doi.org/10.3322/caac.21834
3. Ang K, Harris J, Wheeler R. Human papillomavirus and survival of patients with oropharyngeal cancer. N Engl J Med. 2010;363(1):24–35. https://doi.org/10.1056/NEJMoa0912217
4. Cancer Genome Atlas Network. Comprehensive genomic characterization of head and neck squamous cell carcinomas. Nature. 2015;517(7536):576–582. https://doi.org/10.1038/nature14129
5. Leemans C, Snijders P, Brakenhoff R. The molecular landscape of head and neck cancer. Nat Rev Cancer. 2018;18(5):269–282. https://doi.org/10.1038/nrc.2018.11
6. Ferris R, G B, Fayette J. Nivolumab for recurrent squamous-cell carcinoma of the head and neck. N Engl J Med. 2016;375(19):1856–1867. https://doi.org/10.1056/NEJMoa1602252
7. Burtness B, Harrington K, Greil R. Pembrolizumab alone or with chemotherapy versus cetuximab with chemotherapy for recurrent or metastatic squamous cell carcinoma of the head and neck (KEYNOTE-048): a randomised, open-label, phase 3 study. Lancet. 2019;394(10212):1915–1928.
8. Mandal R, Senbabaoglu Y, Desrichard A. The head and neck cancer immune landscape and its immunotherapeutic implications. JCI Insight. 2016;1(17). https://doi.org/10.1172/jci.insight.89829
9. Khan O, Giles M. *TOX* transcriptionally and epigenetically programs CD8+ T cell exhaustion. Nature. 2019;571(7764):211–218. https://doi.org/10.1038/s41586-019-1325-x
10. Wherry E. T cell exhaustion. Nat Immunol. 2011;12(6):492–499. https://doi.org/10.1038/ni.2035
11. Sade-Feldman M, Yizhak K, Bjorgaard SL, Ray JP, De Boer CG, Jenkins RW, Lieb DJ, et al. Defining T Cell States Associated with Response to Checkpoint Immunotherapy in Melanoma. Cell. 2018 Nov;175(4):998-1013.e20. https://doi.org/10.1016/j.cell.2018.10.038
12. Thorsson V, Gibbs DL, Brown SD, Wolf D, Bortone DS, Ou Yang T, Porta-Pardo E, et al. The Immune Landscape of Cancer. Immunity. 2018 04;48(4):812-830.e14. https://doi.org/10.1016/j.immuni.2018.03.023
13. Cabrita R, Lauss M, Sanna A, Donia M, Skaarup Larsen M, Mitra S, Johansson I, et al. Tertiary lymphoid structures improve immunotherapy and survival in melanoma. Nature. 2020 01;577(7791):561-565. https://doi.org/10.1038/s41586-019-1914-8
14. Fridman WH, Pagès F, Sautès-Fridman C, Galon J. The immune contexture in human tumours: impact on clinical outcome. Nature Reviews Cancer. 2012 04;12(4):298-306. https://doi.org/10.1038/nrc3245
15. Ritchie ME, Phipson B, Wu D, Hu Y, Law CW, Shi W, Smyth GK. limma powers differential expression analyses for RNA-sequencing and microarray studies. Nucleic Acids Research. 2015 04 20;43(7):e47-e47. https://doi.org/10.1093/nar/gkv007
16. Subramanian A, Tamayo P, Mootha VK, Mukherjee S, Ebert BL, Gillette MA, Paulovich A, et al. Gene set enrichment analysis: A knowledge-based approach for interpreting genome-wide expression profiles. Proceedings of the National Academy of Sciences. 2005 Oct 25;102(43):15545-15550. https://doi.org/10.1073/pnas.0506580102
17. Therneau TM, Grambsch PM. Modeling Survival Data: Extending the Cox Model. New York: Springer; 2000.
18. Tibshirani R. Regression shrinkage and selection via the lasso. J R Stat Soc Series B Stat Methodol. 1996;58(1):267–288. https://doi.org/10.1111/j.2517-6161.1996.tb02080.x
19. Friedman J, Hastie T, Tibshirani R. Regularization paths for generalized linear models via coordinate descent. J Stat Softw. 2010;33(1):1–22. https://doi.org/10.18637/jss.v033.i01
20. Blanche P, Dartigues J, Jacqmin-Gadda H. Estimating and comparing time-dependent areas under receiver operating characteristic curves for censored event times with competing risks. Stat Med. 2013;32(30):5381–5397. https://doi.org/10.1002/sim.5958
21. Newman A, Liu C, Green M. Robust enumeration of cell subsets from tissue expression profiles. Nat Methods. 2015;12(5):453–457. https://doi.org/10.1038/nmeth.3337
22. Li Z, Xu W, Kwok HF. Targeting CD39 as a Therapeutic for Cancer Immunotherapy. Expert Reviews in Molecular Medicine. 2026 01 26;28:e5. https://doi.org/10.1017/erm.2026.10033
23. Woo T, ME G. Immune inhibitory molecules LAG-3 and *PD-1* synergistically regulate T-cell function to promote tumoral immune escape. Cancer Res. 2012;72(4):917–927. https://doi.org/10.1158/0008-5472.CAN-11-1620
24. Joller N, Lozano E, Burkett P. Treg cells expressing the coinhibitory molecule *TIGIT* selectively inhibit proinflammatory Th1 and Th17 cell responses. Immunity. 2014;40(4):569–581. https://doi.org/10.1016/j.immuni.2014.02.012
25. She Y, Kong X, Ge Y, Yin P, Liu Z, Chen J. Immune-related gene signature for predicting the prognosis of head and neck squamous cell carcinoma. Cancer Cell Int. 2020;20(22). https://doi.org/10.1186/s12935-020-1104-7
26. Wang Y, Xu Y, Hua Q, Jiang Y, Liu P, Zhang W. Novel prognostic model based on immune signature for head and neck squamous cell carcinoma. Dis Markers. 2020. https://doi.org/10.1155/2020/4725314
27. Qiu Y, Cui L, Lin Y, Gao B, Li J, Zhao X. Development and validation of a robust immune prognostic signature for head and neck squamous cell carcinoma. Front Oncol. 2020;10(1502). https://doi.org/10.3389/fonc.2020.01502
28. Lu Z, Deng X, Li H. Prognostic value of a ten-gene signature in HNSCC patients based on tumor-associated macrophages expression profiling. Front Oncol. 2020;10(569002). https://doi.org/10.3389/fonc.2020.569002
29. Tian Z, Gu Z, Wang X, Li L, Liu B, Wu W. A novel immune-related prognostic signature in head and neck squamous cell carcinoma. Front Genet. 2021;12(614863). https://doi.org/10.3389/fgene.2021.614863
30. Chen L, Cai Z, Lyu K, Cai Z, Lei W. A novel immune-related long non-coding RNA signature improves the prognosis

prediction in the context of head and neck squamous cell carcinoma. Biotechnol Genet Eng Rev. 2021;37(2):152–70. https://doi.org/10.1080/21655979.2021.1943284
31. Chi H, Xie X, Yan Y, Peng G, Strohmer D, Lai G. Natural killer cell-related prognosis signature characterizes immune landscape and predicts prognosis of HNSCC. Front Immunol. 2022;13(1018685). https://doi.org/10.3389/fimmu.2022.1018685
32. Wang C, Zhou Y. Cuproptosis-related gene subtypes predict prognosis in patients with head and neck squamous cell carcinoma. J Otolaryngol Head Neck Surg. 2023;52(1). https://doi.org/10.1186/s40463-023-00655-4
33. Zhang W, Qu M, Yin C, Jin Z, Hu Y. Comprehensive analysis of T cell exhaustion related signature for predicting prognosis and immunotherapy response in HNSCC. Discov Oncol. 2024;15(56). https://doi.org/10.1007/s12672-024-00921-5

This work is licensed under a Creative Commons Attribution-Non Commercial 4.0 International License.